Numerical and analytical estimates of existence regions for semi-linear elliptic equations with critical Sobolev exponents in cuboid and cylindrical domains

C.J. Budd[†] and A.R. Humphries[‡]

8th September 1999

Abstract. We consider the parameterised semi-linear elliptic equation $\Delta u + \lambda u + u^5 = 0, u > 0$, where u is defined to be zero on the boundary of the domain. We perform an analytical study of solutions on cylindrical domains and construct approximate solutions using the finite element method on cuboid domains. This equation is important in analysis and it is known that there is a value $\lambda_0 > 0$ such that no solutions exist for $\lambda < \lambda_0$. McLeod and Schoen, and Bandle and Flucher have given different estimates for λ_0; both of which have been conjectured to be exact. We compute these estimates for cylindrical and cuboid domains, and show that on these domains the estimates do not agree. We conclude that the conjecture of Bandle and Flucher is false. Our numerical computations on cuboid domains are consistent with McLeod's conjecture being true.

Key words. Semi-linear elliptic partial differential equations, finite element method, critical Sobolev exponent, spurious solutions, matched asymptotic expansion.

AMS subject classifications. 35J60, 65N30, 46E35, 65N12, 41A60.

1 Introduction

In [4], Brezis and Nirenberg introduced an interesting class of parametrised semi-linear elliptic partial differential equations which have solutions which develop isolated singularities as the parameter varies. These were given by the system

$$\left.\begin{array}{lll} \Delta u + \lambda u + u^5 = 0, & \text{on } \Omega \subset \mathbb{R}^3, \\ u > 0 & \text{in } \Omega, \\ u = 0 & \text{on } \partial\Omega. \end{array}\right\} \tag{1.1}$$

where Ω is a compact domain in $\mathbb{R}^3$. This problem is of interest both for its applications in differential geometry and also for being a member of a critical class of problems, of great interest in analysis, for which proofs of existence based upon the calculus of variations break down.

For the problem above it is known [4], that there exist certain domains Ω (for example star shaped domains) and a parameter $\lambda_0 > 0$ such that $\|u\|_\infty \to \infty$ as $\lambda \to \lambda_0$ and that no positive solution exists when $\lambda < \lambda_0$. Much of the analysis of this problem has concerned

[†]Department of Mathematical Sciences, University of Bath, Claverton Down, Bath BA2 7AY, UK. Supported by the UK EPSRC through the grants GR/H63456 and GR/J75258.

[‡]Centre for Mathematical Analysis and its Applications, School of Mathematical Sciences, University of Sussex, Brighton, BN1 9QH, UK. Supported by the UK EPSRC through the grants GR/H63456 and GR/J75258.

radially symmetric solutions when Ω is a ball of radius R. In this case (1.1) reduces to an ordinary differential equation, greatly simplifying the analysis and it is known [4] that $\lambda_0 = \pi^2/4R^2$.

In [7] a numerical approximation of the solution of (1.1) in the cube, was constructed using a finite element approximation of u. By obtaining sharp error estimates for this approximation close to the singularity it was possible to extrapolate the numerical solution and to make an accurate calculation of λ_0. Here, we extend these calculations to a numerical study of a one parameter family of square-based cuboid domains Ω_{cub} given by

$$\Omega_{cub} = \{(x,y,z) : -X/2 < x < X/2, -X/2 < y < X/2, -Z/2 < z < Z/2\},$$

and an analytical study of a related family of cylindrical domains Ω_{cyl} given by

$$\Omega_{cyl} = \{(x,y,z) : 0 \leqslant x^2 + y^2 < R^2, -Z/2 < z < Z/2\}.$$

In particular, we seek to find how λ_0 depends upon X, Z and R.

There exist several upper bounds for λ_0. In [4] a variational approach was used to obtain the bound

$$\lambda_0 \leqslant \lambda_* := \frac{\pi^2}{4R^2} \tag{1.2}$$

where Ω contains a sphere of radius R. For Ω a sphere this inequality is an equality, however it is not sharp for general domains, for example the cube [7]. Two further upper bounds for λ_0 have been given, leading to two related conjectures.

1. McLeod [9] and Schoen [12] independently derived an upper bound λ_{**} for λ_0 using the Green's function of the Helmholtz operator, and conjectured that $\lambda_0 = \lambda_{**}$.
2. Bandle and Flucher [2] derive a different upper bound λ_{***}, for λ_0 in terms of the Harmonic Radius of Ω, and conjectured that $\lambda_0 = \lambda_{***}$.

Both of these conjectures are true for the ball but remain unproven for more general domains. The numerical computations presented in this paper are consistent (to numerical accuracy) with Conjecture 1 being *true*. In contrast both analytical and numerical results demonstrate that Conjecture 2 is *false* for a general domain, with $\lambda_{**} < \lambda_{***}$. Though we note that $\lambda_{**} \approx \lambda_{***}$ for all the domains considered.

The first half of this paper looks at the computation of λ_{**} and λ_{***}. In Section 2 we will describe the derivation of McLeod and Schoen's estimate λ_{**} based upon the regular part of the Green's function, and present numerically computed values of λ_{**} on the cuboid domains Ω_{cub} taking the respective limits of X large and Z large. If $\lambda_1(\Omega)$ is defined to be the principle eigenvalue of the negative Laplacian in Ω, then these results support a conjecture of Wang [13] that

$$\frac{1}{4} \leqslant \frac{\lambda_{**}}{\lambda_1} < \frac{4}{9}. \tag{1.3}$$

In Section 3 we will describe the derivation of Bandle and Flucher's estimate λ_{***} based upon the Harmonic Radius, and present numerically computed values of λ_{***} on Ω_{cub}. In Section 4 we compute values of λ_{**} and λ_{***} for the cylindrical domains Ω_{cyl} taking the respective limits of R large, Z fixed and R fixed and Z large. The values of λ_{**}/λ_1 and λ_{***}/λ_1 so obtained are close to the numerically computed results for the cuboid domains computed in the previous two sections. In particular for the case of Z fixed and $R \to \infty$

$$\lambda_{**}/\lambda_1 \to 4/9 = 0.444444444444... < \lambda_{***}/\lambda_1 \to \log^2(2) = 0.48045301392....$$

In the second part of the paper we proceed to calculate λ_0 numerically for the cuboid domains Ω_{cub}. In Section 5 we review the finite element theory underlying our computations and in particular discuss the asymptotic theory behind the error estimates which we use to post process the numerical computations. In Section 6 we then present the numerical computations of the solution of the full nonlinear problem (1.1) on two domains Ω^1_{cub} and Ω^2_{cub} near the limits of the one-parameter family of domains Ω_{cub} considered, where Ω^1_{cub} is a domain with $Z \ll X$, and Ω^2_{cub} is a domain with $X \ll Z$. Using the methods described in Section 5 we then process these computations to obtain estimates for λ_0 and compare these with the estimates λ_{**} and λ_{***} of the previous sections. In [7] we have already presented similar computations for the cube. Together these computations give support for Conjecture 1.

2 Critical values, λ_{**}, derived from the Green's Function of the Helmholtz Operator.

For all of our calculations we will be interested in the limit of λ close to λ_0. Here it is conjectured, with strong numerical support, that as $\lambda \to \lambda_0$ the function $u(\mathbf{x})$ forms an increasing narrow and tall spike at a single point $\mathbf{x} = \mathbf{y}$ with u small elsewhere. Our interest is to find both λ_0 and $\mathbf{y}$. As $u(\mathbf{x})$ forms a narrow spike it is not unreasonable to approximate the function $-u^5(\mathbf{x})$ by the delta function $-\delta(\mathbf{x}-\mathbf{y})$. For this elementary reason we are motivated, on substituting this approximation into (1.1), to study the Green's function for the Helmholtz operator which satisfies the equation

$$\left.\begin{array}{rcll} \Delta G_\lambda(\mathbf{x},\mathbf{y}) + \lambda G_\lambda(\mathbf{x},\mathbf{y}) & = & -\delta(\mathbf{x}-\mathbf{y}), & \mathbf{x} \in \Omega, \\ G_\lambda(\mathbf{x},\mathbf{y}) & = & 0 & \mathbf{x} \in \partial\Omega, \end{array}\right\} \tag{2.1}$$

(where all spacial derivatives are expressed in terms of $\mathbf{x}$). Indeed, formal asymptotic calculations described in [7] indicate that away from a neighbourhood of the peak, u is closely approximated by G_λ. We may write the solution of (2.1) in the form

$$G_\lambda(\mathbf{x},\mathbf{y}) = \frac{1}{4\pi|\mathbf{x}-\mathbf{y}|} + g_\lambda(\mathbf{x},\mathbf{y}) \tag{2.2}$$

where the continuous but non-smooth function $g_\lambda(\mathbf{x},\mathbf{y})$ is called the *regular part* of the Green's function. It follows from (2.1) and (2.2) that

$$\left.\begin{array}{rcll} \Delta g_\lambda(\mathbf{x},\mathbf{y}) + \lambda g_\lambda(\mathbf{x},\mathbf{y}) & = & -\dfrac{\lambda}{4\pi|\mathbf{x}-\mathbf{y}|}, & \mathbf{x} \in \Omega, \\ g_\lambda(\mathbf{x},\mathbf{y}) & = & -\dfrac{1}{4\pi|\mathbf{x}-\mathbf{y}|} & \mathbf{x} \in \partial\Omega. \end{array}\right\} \tag{2.3}$$

Following [3] we define the function

$$\varphi_\lambda(\mathbf{x}) \equiv g_\lambda(\mathbf{x},\mathbf{x}).$$

If $\lambda = 0$ then $-4\pi\varphi(\mathbf{x})$ is called the *Robin's function* of Ω at $\mathbf{x}$. McLeod [9] and Schoen [12] showed independently that if $\varphi_\lambda(\mathbf{x}) > 0$ for some point $\mathbf{x}$ in Ω then (1.1) has a solution. In Brezis [3] it is shown that $\varphi_\lambda(\mathbf{x})$ increases with λ and hence there is a unique $\lambda = \lambda_{**}$ and an $\mathbf{x_0} \in \Omega$ such that

$$\max\{\varphi_\lambda(\mathbf{x}) : \mathbf{x} \in \Omega\} = \varphi_\lambda(\mathbf{x}_0) = 0 \quad \text{if} \quad \lambda = \lambda_{**}.$$

This gives the following result.

Lemma 2.1 *Equation (1.1) has a solution if $\lambda > \lambda_{**}$.* □

McLeod conjectured that $\lambda_{**} = \lambda_0$, with the singularity in $u(\mathbf{x})$ forming at the point $\mathbf{x} = \mathbf{x}_0$. For the unit sphere centred on the origin, $\mathbf{x_0} = \mathbf{0}$ and if $0 < \lambda < \lambda_1$ then $\varphi_\lambda(\mathbf{0}) = -\lambda^{1/2}\cot(\lambda^{1/2})/4\pi$ giving $\lambda_{**} = \lambda_0 = \pi^2/4$. So that the conjecture is true in this case. For less symmetric domains, both $\mathbf{x}_0$ and λ_{**} are hard to determine analytically except in special cases [13]. However, it is clear from this discussion that a numerical computation of the function $g_\lambda(\mathbf{x},\mathbf{y})$ and hence of $\varphi_\lambda(\mathbf{x})$ has the potential of giving much insight into the solutions of (1.1). This computation requires the solution of a linear problem, which can be determined with great accuracy at relatively small cost. However, to determine $\varphi_\lambda(\mathbf{x})$ at a *single* point $\mathbf{x}$ we must calculate $g_\lambda(\mathbf{x},\mathbf{y})$ over the *whole* of the domain Ω. This makes the determination of λ_{**} a formidable task for a domain in which $\mathbf{x}_0$ is not known a-priori. However, in cuboid domains, centred on the origin, symmetry arguments imply that $\mathbf{x_0} = \mathbf{0}$ and hence, we need only consider the function $\varphi_\lambda(\mathbf{0})$ which is a much simpler computational task.

The equation (2.3) has a singularity as $|\mathbf{x}-\mathbf{y}| \to \mathbf{0}$ making computation difficult. Consequently, we solve a related problem which removes this singularity. In contrast to (2.2) we write

$$G_\lambda(\mathbf{x},\mathbf{y}) = \theta_\lambda(\mathbf{x},\mathbf{y}) + h_\lambda(\mathbf{x},\mathbf{y}) \tag{2.4}$$

where

$$\theta_\lambda(\mathbf{x},\mathbf{y}) = \frac{\cos(\lambda^{1/2}|\mathbf{x}-\mathbf{y}|)}{4\pi|\mathbf{x}-\mathbf{y}|}. \tag{2.5}$$

A simple calculation shows that

$$\Delta\theta_\lambda(\mathbf{x},\mathbf{y}) + \lambda\theta_\lambda(\mathbf{x},\mathbf{y}) = -\delta(\mathbf{x}-\mathbf{y}), \tag{2.6}$$

and substituting (2.4) into (2.1) and using (2.6) we obtain

$$\left.\begin{array}{rl} \Delta h_\lambda(\mathbf{x},\mathbf{y}) + \lambda h_\lambda(\mathbf{x},\mathbf{y}) = 0, & \mathbf{x}\in\Omega, \\ h_\lambda(\mathbf{x},\mathbf{y}) = -\theta_\lambda(\mathbf{x},\mathbf{y}) & \mathbf{x}\in\partial\Omega. \end{array}\right\} \tag{2.7}$$

If $y \notin \partial\Omega$ then the function θ_λ is smooth on the boundary of $\partial\Omega$. Thus, if $\lambda < \lambda_1$, standard results from the theory of elliptic partial differential equations predict that the function h_λ exists and (unlike g_λ), is smooth in the interior of Ω. Finally, using (2.2) and (2.4) it follows that

$$\begin{aligned} g_\lambda(\mathbf{x},\mathbf{y}) &= \theta_\lambda(\mathbf{x},\mathbf{y}) - \frac{1}{4\pi|\mathbf{x}-\mathbf{y}|} + h_\lambda(\mathbf{x},\mathbf{y}) \\ &= \frac{1}{4\pi|\mathbf{x}-\mathbf{y}|}\Big(\cos(\lambda^{1/2}|\mathbf{x}-\mathbf{y}|) - 1\Big) + h_\lambda(\mathbf{x},\mathbf{y}) \end{aligned} \tag{2.8}$$

Letting $\mathbf{x} \to \mathbf{0}$ in (2.8) then gives

$$\varphi_\lambda(\mathbf{0}) = g_\lambda(\mathbf{0},\mathbf{0}) = h_\lambda(\mathbf{0},\mathbf{0}). \tag{2.9}$$

To compute λ_{**} for cuboid domains with $\mathbf{x_0} = \mathbf{0}$ we solve (2.7) for $h_\lambda(\mathbf{x},\mathbf{0})$ using the finite element method on a regular cubic mesh and tri-linear basis functions. The value of λ_{**} is determined by using path following in λ and interval bisection to find the unique value of λ_{**} such that $\varphi_{\lambda_{**}}(\mathbf{0}) = 0$. We note that as the function h_λ is smooth, standard error estimates from the theory of the finite element method may be applied to determine the accuracy of this computation. As the value of θ_λ on $\partial\Omega$ depends smoothly upon λ, as does the inverse of the linear operator in (2.8) the constants implied in these calculations (unlike those in the calculation of the nonlinear equation) are largely independent of λ, and consequently we predict a consistently accurate solution. The results are shown in the following table for a variety of cuboids of different aspect ratio. A simple calculation shows that for these domains

$$\lambda_1 = \pi^2 \left(\frac{2}{X^2} + \frac{1}{Z^2} \right),$$

and for clarity of presentation, we have scaled X and Z so that $\lambda_1 = 3\pi^2$ is the same for each. The calculations are also presented in Figure 1 where we plot the ratio of λ_{**}/λ_1 against the aspect ratio Z/X of the box.

X	Z	Grid	λ_{**}	λ_{**}/λ_1
∞	0.57735		13.15947	0.444444
$\uparrow$	$\uparrow$		$\uparrow$	$\uparrow$
8.55163	0.58	$240 \times 240 \times 20$	13.02671	0.439961
3.96429	0.59	$170 \times 170 \times 26$	12.59593	0.425412
3	0.6	$150 \times 150 \times 30$	12.18133	0.411409
1.77732	0.65	$132 \times 132 \times 44$	10.45127	0.352978
1.44399	0.7	$120 \times 120 \times 60$	9.280753	0.313446
1.17954	0.8	$100 \times 100 \times 70$	8.052492	0.271963
1.06436	0.9	$100 \times 100 \times 84$	7.603195	0.256788
1	1	$100 \times 100 \times 100$	7.503829	0.253432
0.931381	1.2	$92 \times 92 \times 118$	7.685691	0.259574
0.884652	1.5	$84 \times 84 \times 144$	8.121561	0.274295
0.852803	2	$74 \times 74 \times 170$	8.632497	0.291551
0.821995	5	$54 \times 54 \times 330$	9.279121	0.313391
0.817861	10	$42 \times 42 \times 530$	9.371609	0.316514
0.816837	20	$34 \times 34 \times 840$	9.392950	0.317234
0.816551	50	$26 \times 26 \times 1300$	9.393971	0.317269
$\downarrow$	$\downarrow$			
0.816497	∞			

We note a number of interesting features from these results. Firstly, for all domains considered the ratio λ_{**}/λ_1 satisfies the conjecture (1.3) of Wang [13], and in the limit as $Z/X \to 0$ the computed value of λ_{**}/λ_1 is converging to 4/9 as required by Wang's result [13] that if $E_{s,B} = \{x \in \mathbb{R}^3 : -s < x_1 < s, (x_2, x_3) \in B\}$ where B is any bounded domain then as $s \to 0$

$$\frac{\lambda_{**}(E_{s,B})}{\lambda_1(E_{s,B})} \to \frac{4}{9}.$$

Notice also that λ_{**}/λ_1 takes a minimum value slightly greater than 1/4 for the cube when $X = Y = Z = 1$. This is to be expected since in the family of domains considered the cube has the most symmetry and is closest to the case of a sphere for which it is known analytically that $\lambda_{**}/\lambda_1 = 1/4$. Note also from the table that λ_{**}/λ_1 appears to tend to a limit as the aspect ratio $Z/X \to \infty$. The value of this limit will be determined by quadrature in Section 4.

3 Critical values, λ_{***}, derived from the Harmonic Radius

A second conjecture on the value of λ_0 is presented in [2] where it is bounded in terms of the Harmonic Radius $r(\mathbf{x})$ of the domain Ω at the point $\mathbf{x}$, which, using the notation of

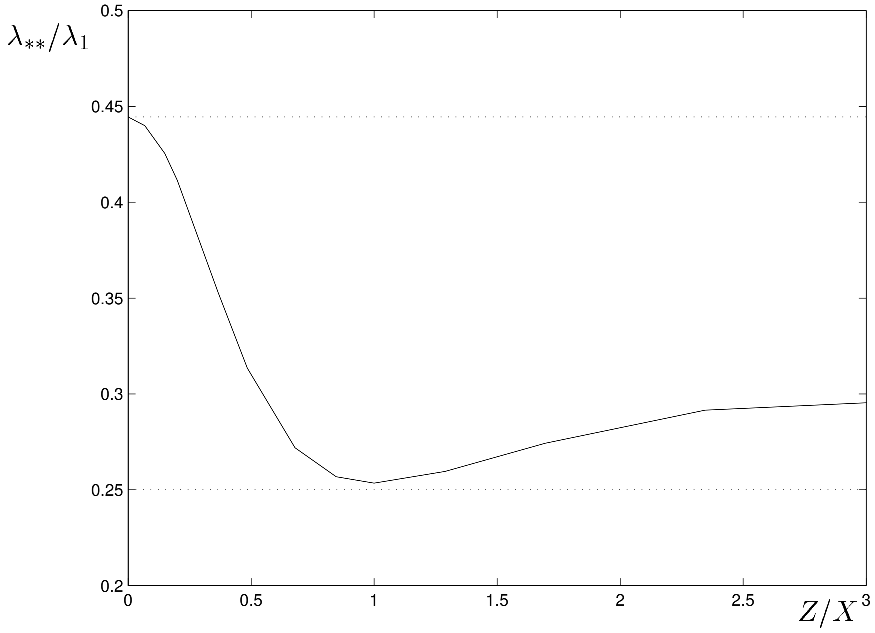

Figure 1: Graph of λ_{**}/λ_1 against the aspect ratio Z/X of the box.

Section 2, is given by

$$r(\mathbf{x}) = -\frac{1}{4\pi\varphi_0(\mathbf{x})}. \tag{3.1}$$

Point(s) where $r(\mathbf{x})$ is at a maximum are called *Harmonic Centre(s).* A review of the properties of the Harmonic Radius and the Harmonic Centre is given in [2]. Since $\varphi_0(\mathbf{x}) < 0$ for all $\mathbf{x} \in \Omega$, both $\varphi_0(\mathbf{x})$ and $r(\mathbf{x})$ take their maximum values at the same point, which by symmetry must be the centre of the cuboid. (In [2] it is quoted that for a convex domain such as a cuboid then it is expected that there is a unique harmonic centre which must be at the centre.) Thus to compute $\max(r(\mathbf{x}))$, by (2.9), it is sufficient to compute $h_0(0,0)$. Note that this leads to a much simpler numerical computation than in Section 2, since in this section all our computations are performed with $\lambda = 0$, and we do not require interval bisection. By using the process of harmonic transplantation, Bandle and Flucher obtained the following upper bound for λ_0 for domains with a bounded harmonic radius.

Theorem 3.1 *Let $r = max(r(\mathbf{x}))$ then*

$$\lambda_0 \leqslant \frac{\pi^2}{4r^2}. \qquad \square$$

Defining

$$\lambda_{***} = \frac{\pi^2}{4r^2} \tag{3.2}$$

leads to the the conjecture

$$\lambda_0 = \lambda_{***}. \tag{3.3}$$

For a symmetric domain centred on the origin we have

$$\lambda_{***} = 4\pi^4\varphi_0(\mathbf{0})^2 \tag{3.4}$$

and this value can be computed easily using the methods of the previous section. The results so obtained are displayed in the following table for the same cuboid domains and associated meshes as were used in the previous section.

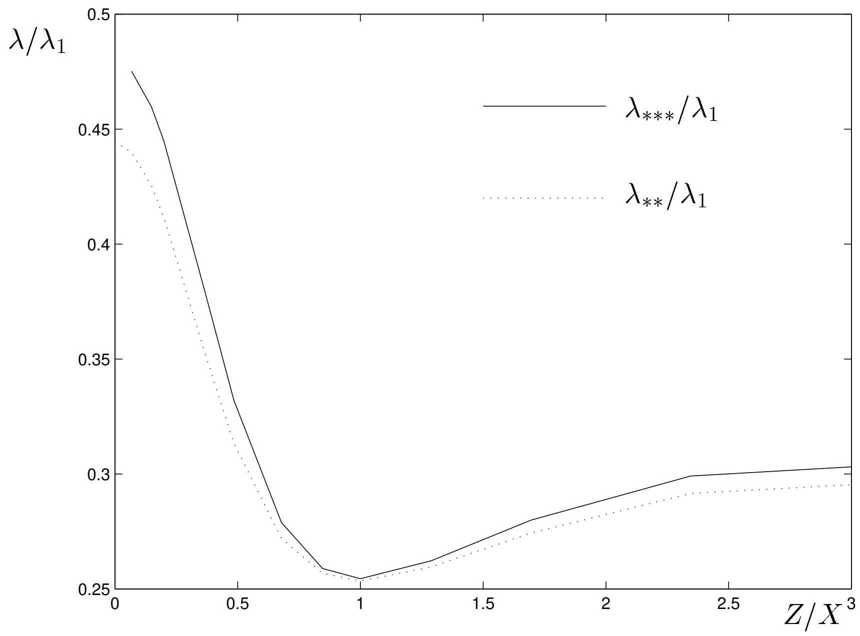

Figure 2: Graph of λ_{**}/λ_1 and λ_{***}/λ_1 against the aspect ratio Z/X of the box.

X	Z	Grid	λ_{***}	λ_{***}/λ_1
∞	0.57735			
$\uparrow$	$\uparrow$			
8.55163	0.58	$240 \times 240 \times 20$	14.07009	0.4752
3.96429	0.59	$170 \times 170 \times 26$	13.61103	0.4597
3	0.6	$150 \times 150 \times 30$	13.16400	0.4446
1.77732	0.65	$132 \times 132 \times 44$	11.24027	0.3796
1.44399	0.7	$120 \times 120 \times 60$	9.832192	0.3321
1.17954	0.8	$100 \times 100 \times 70$	8.256828	0.2789
1.06436	0.9	$100 \times 100 \times 84$	7.665089	0.2589
1	1	$100 \times 100 \times 100$	7.534445	0.2545
0.931381	1.2	$92 \times 92 \times 118$	7.765307	0.2623
0.884652	1.5	$84 \times 84 \times 144$	8.289288	0.2800
0.852803	2	$74 \times 74 \times 170$	8.856933	0.2991
0.821995	5	$54 \times 54 \times 330$	9.527840	0.3218
0.817861	10	$42 \times 42 \times 530$	9.622361	0.3250
0.816837	20	$34 \times 34 \times 840$	9.643693	0.3257
0.816551	50	$26 \times 26 \times 1300$	9.643702	0.3257
$\downarrow$	$\downarrow$			
0.816497	∞			

In Figure 2 we plot both the values of λ_{***} computed here and the values of λ_{**} from Section 2 against the aspect ratio Z/X of the domain. Clearly $\lambda_{***} > \lambda_{**}$ for all domains considered. This gives numerical evidence for the conclusion that Bandle and Flucher's conjecture that $\lambda_0 = \lambda_{***}$ is *false*.

4 Cylindrical Domains

In this section we make some analytic calculations of λ_{**} and λ_{***} for the following two cylindrical domains

$$\Omega^1_{cyl} = \{(x, y, z) : x^2 + y^2 < R^2, \quad -1/2 < z < 1/2\}$$

and

$$\Omega^2_{cyl} = \{(x, y, z) : x^2 + y^2 < 1, \quad -Z/2 < z < Z/2\},$$

considering the respective limits of R large and Z large. These two limits correspond to considering cuboid domains with X large or Z large respectively. Trivially we have that in the limit of $R, Z \to \infty$

$$\lambda_1(\Omega^1_{cyl}) = \pi^2 \quad \text{and} \quad \lambda_1(\Omega^2_{cyl}) = j_1^2 = 5.78318596292$$

where j_1 is the first zero of the Bessel function $J_0(x)$.

4.1 The domain Ω^1_{cyl}

The calculation of λ_{**} for Ω^1_{cyl} was considered in detail by Wang [13]. In particular Wang showed that as $R \to \infty$

$$\varphi_\lambda(\mathbf{0}) = \frac{1}{2\pi} \sum_{k=1}^{\infty} (-1)^k \frac{\cos(k\sqrt{\lambda})}{k} = -\frac{1}{2\pi} \log\left(2\cos\left(\frac{\sqrt{\lambda}}{2}\right)\right).$$

Hence

$$\varphi_\lambda(\mathbf{0}) = 0 \quad \text{if} \quad \lambda_{**} = \frac{4}{9}\pi^2 \quad \text{so that} \quad \lambda_{**}/\lambda_1 = 4/9 = 0.4444444....$$

Using this result we also have

$$\varphi_0(\mathbf{0}) = -\frac{1}{2\pi}\log(2)$$

and hence

$$\lambda_{***} = \log^2(2)\pi^2 \quad \text{so that} \quad \lambda_{***}/\lambda_1 = \log^2(2) = 0.48045301392....$$

Comparing these value with those in Tables 2.1, 3.1 we see that the limits of λ_{**}/λ_1 and λ_{***}/λ_1 for the cuboid domains with Z fixed and $X \to \infty$, approach values close to the limits above. This is precisely to be expected, as (following the argument in [13]) each such cuboid domain can be bounded both inside and outside by a corresponding cylindrical domain provided that R is sufficiently large. From this calculation it is clear that for the domain Ω^1_{cyl}

$$\lambda_{**} < \lambda_{***}.$$

4.2 The domain Ω^2_{cyl}

In this case we compute the critical values of λ by using Fourier transforms in z. Setting $r^2 = x^2 + y^2$ and seeking radially symmetric solutions $h(r, z)$ of (2.7), we have that

$$h_{rr} + \frac{1}{r}h_r + h_{zz} + \lambda h = 0, \quad h_r(0, z) = 0, \tag{4.1}$$

and

$$-4\pi h(1, z) = \frac{\cos(\sqrt{\lambda}\sqrt{1 + z^2})}{\sqrt{1 + z^2}}. \tag{4.2}$$

A general solution of the differential equation (4.1) is given by

$$h(r,z) = \int_0^{\sqrt{\lambda}} a(\omega) J_0(\sqrt{\lambda-\omega^2}\quad r)\cos(\omega z)d\omega + \int_{\sqrt{\lambda}}^{\infty} b(\omega) I_0(\sqrt{\omega^2-\lambda}\quad r)\cos(\omega z)d\omega \tag{4.3}$$

where $J_0(x)$ and $I_0(x)$ are the regular and modified Bessel functions of the first kind [1]. The Fourier transform of the right hand side of (4.2) is given on page 737 of [8] and from this we have

$$4\pi h(1,z) = \int_0^{\sqrt{\lambda}} Y_0(\sqrt{\lambda-\omega^2})\cos(\omega z)d\omega - \frac{2}{\pi}\int_{\sqrt{\lambda}}^{\infty} K_0(\sqrt{\omega^2-\lambda})\cos(\omega z)d\omega, \tag{4.4}$$

where $Y_0(x)$ and $K_0(x)$ are the regular and modified Bessel functions of the second kind [1]. Setting $r=1$ and comparing terms in (4.3) and (4.4) gives

$$4\pi a(\omega) = \frac{Y_0(\sqrt{\lambda-\omega^2})}{J_0(\sqrt{\lambda-\omega^2})} \quad \text{and} \quad 4\pi b(\omega) = -\frac{2}{\pi}\frac{K_0(\sqrt{\omega^2-\lambda})}{I_0(\sqrt{\omega^2-\lambda})}.$$

Substituting into (4.3) and setting $r=z=0$ then gives

$$4\pi\varphi_\lambda(\mathbf{0}) = \int_0^{\sqrt{\lambda}} \frac{Y_0(\sqrt{\lambda-\omega^2})}{J_0(\sqrt{\lambda-\omega^2})}d\omega - \frac{2}{\pi}\int_{\sqrt{\lambda}}^{\infty}\frac{K_0(\sqrt{\omega^2-\lambda})}{I_0(\sqrt{\omega^2-\lambda})}d\omega. \tag{4.5}$$

Both of the integrands in (4.5) have a mild logarithmic singularity at $\omega = \sqrt{\lambda}$ but are otherwise regular. Furthermore, the second integrand converges exponentially rapidly to zero as $\omega \to \infty$. The integrals can thus both be evaluated readily using numerical quadrature. To do this we use a Clenshaw-Curtis quadrature algorithm [11] which is particularly suited for problems with logarithmic singularities. The particular implementation of this algorithm used was that given in the NAG routines D01APF, D01AMF with the NAG routines S18ACF and S18CEF used to compute the appropriate Bessel functions [10]. Having computed the integrals, the value of λ for which $\varphi_\lambda(\mathbf{0}) = 0$ was determined by bisection. This calculation gives

$$\varphi_\lambda(\mathbf{0}) = 0 \quad \text{if} \quad \lambda_{**} = 1.8258462960.$$

In the case of $\lambda = 0$, (4.5) simplifies to

$$-2\pi^2\varphi_0(\mathbf{0}) = \int_0^{\infty}\frac{K_0(\omega)}{I_0(\omega)}d\omega. \tag{4.6}$$

Evaluating this integral using the method above then gives

$$-2\pi^2\varphi_0(\mathbf{0}) = 1.3676768619 \quad \text{so that} \quad \lambda_{***} = 1.36767686191^2 = 1.8705399986$$

For the infinite cylinder $\lambda_1 = j_1^2$ and hence

$$\lambda_{**}/\lambda_1 = 0.315716338312 \quad \text{and} \quad \lambda_{***}/\lambda_1 = 0.323444553.$$

These values compare well with the limiting values obtained for the cuboid domains with X fixed and $Z \to \infty$. We see again that for this domain

$$\lambda_{**} < \lambda_{***}.$$

However, we observe that for both Ω^1_{cyl} and Ω^2_{cyl} the value of λ_{**} is close to λ_{***}.

5 Finite Element Computations on the Full Nonlinear Problem.

5.1 Asymptotic theory

We now proceed to calculate λ_0 for the cuboid domains. This calculation is similar to that reported for the cube in [7] and we refer the reader to this paper for more details whilst giving a sketch of the methods here. The aim of these calculations is to reproduce accurately the behaviour of the solutions of (1.1) as $\lambda \to \lambda_0$ identifying λ_0 as the value of λ at which $\sup(u) \to \infty$. Asymptotic analysis of u for these values given in [7] implies that if $\sup(u) = \gamma$ then u has a peak centred at the origin of width $\mathcal{O}(\gamma^{-2})$ where $\gamma = \mathcal{O}(\lambda - \lambda_0)^{-1/2}$.

To perform our calculations we use the finite element method with a fine mesh of regular cubes of side h close to the centre of the domain, where the solution is large, and a coarser mesh of cuboid elements closer to the boundary. For a finite element basis we use piecewise linear functions defined on this mesh. The solution $u(\mathbf{x})$ of the partial differential equation is then approximated by the piecewise linear function $U_h(\mathbf{x})$ defined on the mesh and which satisfies the weak form of (1.1) defined on the finite dimensional space S_h spanned by the basis functions. There are three main problems in using such a finite element discretisation.

1. As the domains are three dimensional, relatively coarse meshes lead to a nonlinear algebraic problem with a large number of unknowns. If a Newton-Raphson method is used to solve this, the solution of the linear systems is hard.

2. The narrowness of the peak implies that we can only hope to resolve any structure if the cubes close to the centre are small. A naive analysis based upon the length scales of the peak would imply that if the cubes have side h then we should have $h = \mathcal{O}(\gamma^{-2})$. In fact the analysis presented in [7] shows owing to the special singular nature of the problem, that to maintain a small error we require that $h = \mathcal{O}(\gamma^{-4})$. Even for moderate values of γ say $\gamma = 10$ this places a significant restriction on the mesh size. In [5] an adaptive approach is considered in an attempt to reduce the computational cost. However this is still very expensive as to cover the support of the peak with the fine mesh we require $\gamma^{-2}/\gamma^{-4} = \gamma^2$ cubes close to the origin, regardless of the size of the cuboids close to the boundary.

3. A subtle feature of our approach is the fact that it can be proven (using the mountain pass theorem) [7], that whilst the continuous equation (1.1) has no positive solution for $\lambda < \lambda_0$ the discrete finite element equations (on a fixed ie. non-adaptive) mesh have solutions for *all* $\lambda < \lambda_1$. Thus any positive solution computed for $\lambda < \lambda_0$ is spurious and misleading to the computation.

Despite these inherent difficulties, it was shown in [7], [6] that provided $\gamma^2 h \ll 1$ and a regular mesh of cubes is used close to the peak, then there is sufficient regularity in the discretisation to allow the establishment of asymptotic scaling laws for the discrete solution. In particular the following formal results are established in the above papers by using matched asymptotic methods based upon rescaling arguments.

Formal Proposition 5.1 *Suppose that* $\gamma = \sup(U_h(\mathbf{x}))$, $\Gamma = \sup(u(\mathbf{x}))$ *with* $\gamma \gg 1, \Gamma \gg 1$. *Furthermore, suppose that* h *is sufficiently small so that* $\gamma^2 h \ll 1$ *then* *(a) if* $\lambda = \lambda_0$*, there is a constant* C *which depends upon the elements used (for cubic elements* $C = 0.0018674..$ *such that*

$$\gamma \approx \left(\frac{\lambda_0}{C}\right)^{1/8} h^{-1/4}, \tag{5.1}$$

with similar behaviour observed for $\lambda < \lambda_0$.
(b) If $\lambda > \lambda_0$ *then*

$$\frac{(\Gamma - \gamma)}{\gamma} \approx \frac{C\gamma^8 h^2}{2\lambda} \tag{5.2}$$

and

$$\Gamma \approx \gamma^*(\gamma, h) = \frac{\gamma}{\sqrt{1 - Ch^2\gamma^8/\lambda}}. \tag{5.3}$$

□

We see the effects of spuriosity in (5.1). Observe that a discrete solution exists when $\lambda = \lambda_0$ but that this solution becomes infinite (slowly) as $h \to 0$. In (5.2) we see that the error is large if γ is large. The result (5.3) is most useful. It allows us to post-process the results of the calculation so that given an approximation γ to Γ a much better approximation γ^* can be found by applying (5.3). This procedure was used very successfully in [7] and [6]. It should be emphasised that the asymptotic results above which were derived in [7] for the cube, apply equally well for cuboid domains, provided that a regular mesh of cubes is used close to the origin. However, their accuracy also depends upon the mesh used away from the origin, which for the cuboid comprises elongated elements.

5.2 Implementation and Performance

The basic implementation of the finite element method with regular cubic meshes to solve (1.1) on cubic domains was described in [7], and we will not repeat the details here. The only difference in the implementation here, for solving on cuboid domains, is that we also consider irregular but topologically regular meshes. These meshes are obtained by slicing the domain in the 3 planes perpendicular to the planes defined by the coordinates axes. If the slices are all equal this results in a regular mesh. However the theory of Section 5.1 allows us to compute more accurate solutions with the same number of elements by having finer elements near the centre of the domain and coarser elements near the boundaries. Thus in each coordinate direction we take regular narrow slices near the centre of the domain and regular wider slices near the boundaries. Such a mesh is shown in Figure 3. Note that the mesh is always set up to have a fine regular array of cubic elements around the centre of the domain, with a node at the centre of the domain. Near the corners of the domain we have a regular array of coarse elements. These elements are also cubic for the domain Ω^1_{cub} below, but are only roughly cubic for the domain Ω^2_{cub} (which has an irrational aspect ratio). Note that near the centres of the faces of the domain cuboid elements with bad aspect ratios may result. The effect of these on the computation is studied below.

Solutions are computed by path following in λ. At each value of λ, by extrapolating from the solutions at the two previously computed (nearby) values of λ, we obtain a very good initial approximation to the solution, and so a variant of Newton's method is appropriate to find the solution. Newton's method itself is inappropriate because the meshes we use are so large (10^6 elements) that, even using sparse storage techniques, it would require several Gigabytes of RAM to store the Jacobian matrix. Thus we use an

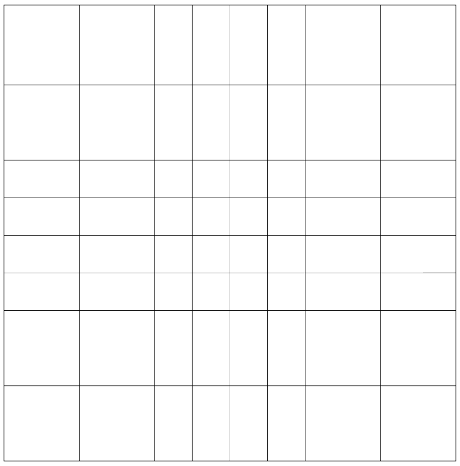

Figure 3: Two-dimensional Projection of a Topologically Regular Mesh

approximation to the Jacobian matrix which results in an approximate Newton's method. This approximation uses an element-by-element sparse storage structure and exploits the fact that the terms in the Jacobian resulting from the linear terms in (1.1) are independent of U_h and only depend on the element's geometry, and since we use topologically regular meshes we only have a very small number of different elements and so this part of the Jacobian can be stored very cheaply. To deal with the nonlinear terms in the Jacobian resulting from the u^5 term we diagonalise the resulting element sub-matrices similar to product approximation (but note that our approach differs from product approximation in that we do not modify the equations to be solved). This approach would work well if U_h was smooth with $0 < U_h \ll 1$, but unfortunately as $\lambda \to \lambda_0$, U_h develops a 'spike' at the centre of the domain, and so neither condition is satisfied, and the Newton iteration fails to converge with this approximation. However, away from the centre of the domain U_h *is* smooth with $0 < U_h \ll 1$, and so we adopt the approach of using product approximation to diagonalise the sub-matrices corresponding to elements away from the centre of the domain, whilst using Gaussian quadrature to exactly compute the element sub-matrices near to the centre of the domain. In practice, it is sufficient to do the full computation over only 10^3 of the 10^6 elements, and our approximate Jacobian matrix retains the symmetry of but only requires $1/36$ of memory of the exact Jacobian. Although, we lose the quadratic convergence of Newton's method, by using the approximate Jacobian, because we have a good initial approximation to the solution and our approximate Jacobian has very similar action to the Jacobian we obtain fast linear convergence with convergence constant k typically between 10^{-2} and 10^{-3}.

At each step of the Newton iteration we need to invert the approximate Jacobian matrix, and we do this using an un-preconditioned conjugate gradient (CG) iteration. Although the CG method is only robust for positive definite problems, and our Jacobian matrix is mildly indefinite no convergence problems were observed, and CG consistently outperformed a MINRES iteration which is robust in this situation. We did not use pre-conditioning as simple ILU pre-conditioners cannot be used as we only have a sparse representation of the matrix, moreover the indefiniteness means that many standard pre-conditioners do not improve the computation, and finally the convergence of the un-preconditioned CG was found to be adequate.

With a CG iteration nested within a Newton iteration for the sake of efficiency some care needs to be taken in the choice of the CG tolerance. The initial guess for the CG update is taken to be **0** and so has the same residual as the approximate solution from the Newton iteration. Now since we are using an approximate Jacobian matrix which will only give the Newton update accurate to several significant figures, there is no point in computing these updates to a higher accuracy than this, and so we use a CG tolerance which is based on the Newton update residual multiplied by a factor (usually 0.003). This was found to save many thousands of CG iterations compared to using an absolute CG tolerance over the length of the path following interval, and did not degrade the convergence of the approximate Newton iteration.

The following table details run-time data that allows us to consider the efficiency of this implementation. Three separate computations with different regular meshes on the domain Ω^1_{cub} are displayed. (The results of these computations are described in Section 6.1 below.)

Mesh	Elements	Newton its	CG its	CGs per N	Time
$50 \times 50 \times 10$	2.5×10^4	241	6887	28.6	48m 33s
$100 \times 100 \times 20$	2.0×10^5	213	10948	51.4	11h 23m 17s
$150 \times 150 \times 30$	6.75×10^5	215	16448	76.5	44h 13m 9s

These computations use path following from the bifurcation point $\lambda = \lambda_1$ to $\lambda = 0$ with $\boldsymbol{U}_h$ computed at each of 60 different values of λ. Thus for the $150 \times 150 \times 30$ mesh the computation involved finding 643829 unknowns to define $\boldsymbol{U}_h$ 60 times. At each value of λ on average only 3.63 Newton iterations were required with 76.5 CG iterations per Newton iteration. Nevertheless in total this results in 16448 CG iterations over the whole computation which took 44 hours on a single 200MHz processor 192MB RAM Silicon Graphics Indy.

To consider the effect of the elements with bad aspect ratios which arise in the topologically regular meshes we will consider the $132 \times 132 \times 60$ mesh used in Section 6.1. Noting above that the total number of Newton iterations for the regular meshes is roughly constant whilst the number of CG iterations is proportional to $N_{els}^{1/3}$ where N_{els} is the number of elements, and also since most of the time in the matrix vector multiplication (which takes most of the time in the CG iteration) is taken in multiplying by the stiffness matrices and this work is proportional to N we can make the following estimates. Firstly if the poor aspect ratios had no affect on the performance of the algorithm since the $132 \times 132 \times 60$ mesh has 1.5488 times more elements than the $150 \times 150 \times 30$ mesh we would expect the computation to need $1.5488^{1/3} \times 16448 = 19030$ CG iterations and to take $1.5488^{4/3} \times 44 = 79$ hours. Secondly, if we had used a regular $300 \times 300 \times 60$ mesh which has the same fineness at the centre of the domain as the irregular mesh we would expect it to take $2 \times 16448 = 32896$ CG iterations and $2^4 \times 44 = 704$ hours. The actual computation required 229 hours and 69038 CG iterations. Thus this computation is much faster than the computation on the regular mesh would be if it were possible (we have insufficient memory to perform such a computation), but requires roughly a factor of 10/3 more time and CG iterations than a regular mesh with the same number of elements; 10/3 being the aspect ratio of the worst elements in this mesh.

If it were necessary to compute the full length of the bifurcation branch from λ_1 to the value of λ at which we required a solution on each mesh the computations would be prohibitively expensive, however this is not necessary. Given an estimate of $\|U_h\|_\infty$ for any value of λ away from the bifurcation point λ_1 (from a computation on a coarser mesh for example) we can compute $\boldsymbol{U}_h(\mathbf{x})$ over the entire mesh for this value of λ very quickly, and subsequently path follow from this solution if required. In [7] it is argued that at the centre of the domain $U_h(\mathbf{x})$ is close to $w_\gamma(\mathbf{x})$ where

$$w_\gamma(\mathbf{x}) = \frac{\gamma}{(1+\frac{1}{3}\gamma^4|x|^2)^{1/2}}$$

with $\gamma = \|U_h\|_\infty$ is a solution of the Cauchy problem $\Delta u + u^5 = 0$. In fact the agreement between $w_\gamma(\mathbf{x})$ and $U_h(\mathbf{x})$ is so good that for a given value of λ we can use $w_\gamma(\mathbf{x})$ with an approximate value of $\|U_h\|_\infty$ to start the numerical computation. Even for moderate values of γ, we have $0 < w_\gamma(\mathbf{x}) < 1$ on $\partial\Omega$ so that although the initial approximation is not good here for both the initial approximation and the solution $0 < u^5 \ll 1$ so that the u^5 term does not make a significant contribution, and near to $\partial\Omega$ the problem is essentially linear, and Newton's method converges in one iteration on linear problems. Meanwhile, $w_\gamma(\mathbf{x})$ is a good approximation to U_h near to the centre of the domain, and so on reflection it is not surprising that the approximate Newton iteration converges rapidly to the solution branch in this case.

6 Results

6.1 Numerics on a short fat domain: Ω^1_{cub}

In this section we present numerical computations for the full nonlinear problem (1.1) on the cuboid domain Ω^1_{cub} for which $X = 3$ and $Z = 0.6$ so that X is rather larger than Z. The computations described are carried out on fixed topologically regular meshes with cuboid elements all of whose edges are aligned with the coordinate axes. For coarse mesh computations we use regular meshes with cubic elements. We are limited by computational power to meshes of at most approximately 10^6 elements. However we obtain more accurate computations without increasing the number of elements by using a mesh which concentrates more elements near to the centre of the domain where the numerical solution develops a spike. We do this in the simplest possible way, using a mesh which is irregular, but topologically regular, obtained by slicing the domain in the 3 planes perpendicular to the planes defined by the coordinates axes. We take regular fine slices over the centre of the domain, so as to obtain a regular cubic mesh over a central cuboid core of the domain, with regular but coarser slices over the rest of the domain to give coarser cuboid elements. The meshes uses are given in the following table.

Core	Core Mesh	Core h	Complete Mesh	'h'
$3 \times 3 \times 0.6$	$50 \times 50 \times 10$	0.06	–	–
$3 \times 3 \times 0.6$	$100 \times 100 \times 20$	0.03	–	–
$3 \times 3 \times 0.6$	$150 \times 150 \times 30$	0.02	–	–
$0.6 \times 0.6 \times 0.6$	$40 \times 40 \times 40$	0.015	$160 \times 160 \times 40$	0.02
$0.6 \times 0.6 \times 0.6$	$50 \times 50 \times 50$	0.012	$146 \times 146 \times 50$	0.025
$0.6 \times 0.6 \times 0.6$	$60 \times 60 \times 60$	0.01	$132 \times 132 \times 60$	0.0333
$0.6 \times 0.6 \times 0.6$	$70 \times 70 \times 70$	0.0086	$122 \times 122 \times 70$	0.0462
$0.45 \times 0.45 \times 0.6$	$60 \times 60 \times 80$	0.0075	$116 \times 116 \times 80$	0.0455

The first column of the table gives the size of the central core of the domain on which we use a cubic mesh, the second column gives the mesh used on this central core displayed as the number of elements in each coordinate direction, and the third column the resulting mesh size h across the core. The three coarsest meshes are regular. For the finer irregular meshes the fourth column gives the mesh used across the whole domain, again displayed as

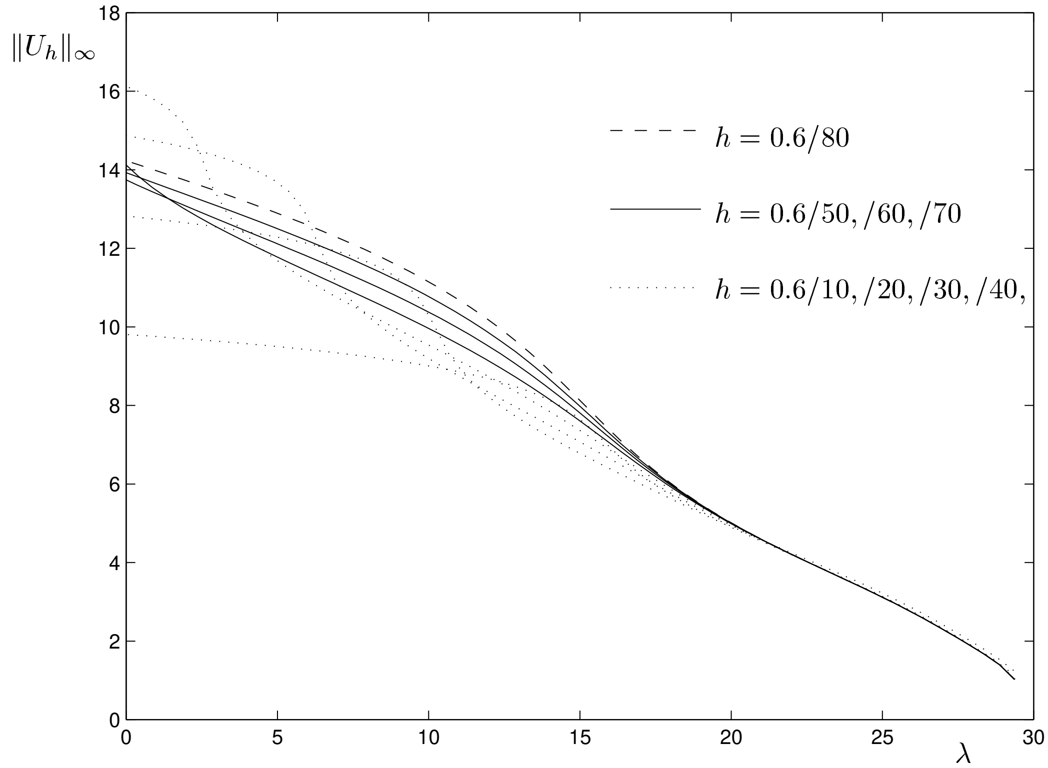

Figure 4: Graph of $\|U_h\|_\infty$ against λ for various meshes on the domain Ω^1_{cub}.

the number of elements in each coordinate direction, and the final column gives the mesh size h given as the largest length of a side of an element. Thus for example, the fourth mesh has three different shaped elements; all elements in the central core are cubic of side length 0.015, whilst elements which are not in the central core are either $0.015 \times 0.02 \times 0.015$, $0.02 \times 0.015 \times 0.015$ or $0.02 \times 0.02 \times 0.015$. Note that on the finer meshes this results in elements with progressively worse aspect ratios (where the aspect ratio is given by dividing the two values of h given in the table). However, since the numerical solution is close to zero uniformly across the elements with bad aspect ratios (since they are not at the centre of the domain), they do not affect the computation adversely. Finally, we emphasise that for each of the irregular meshes there are two different measures of h in the table, which have different functions. The value of h given in the third column gives the mesh size across the central core where the numerical solution develops a spike. It is this measure of h which is used in the asymptotic theory of Section 5, and hence we see structure in the convergence pattern of Figure 4 as this measure of h is refined.

In Figure 4 we plot the infinity norm of the numerical solution U_h against λ on various meshes. The resulting graph has a similar structure to the graphs in [7] for the cube. Note that on the course meshes $h \geqslant 0.6/40$ for which $h\gamma^2$ is not small, there is little agreement between the numerical solutions on the different meshes for $\lambda \leqslant 20$, which indicates that the numerical solutions on these meshes are highly inaccurate. On the finer meshes $h < 0.6/40$ there is better agreement for $15 \leqslant \lambda \leqslant 20$ whilst for lower values of λ it appears that $\|U_h\|_\infty$ is increasing monotonically as h is refined. Indeed for $0 \leqslant \lambda < \lambda_0$ we showed in Section 5 that $\|U_h\|_\infty \to \infty$ as $h \to 0$ but that since from (5.1) $\|U_h\|_\infty = \mathcal{O}(h^{-1/4})$ it follows that $\|U_h\|_\infty$ is only increasing very slowly as h is refined. Moreover, the convergence of $\|U_h\|_\infty$ to the exact value $\|u\|_\infty$ given by (5.2) is also very

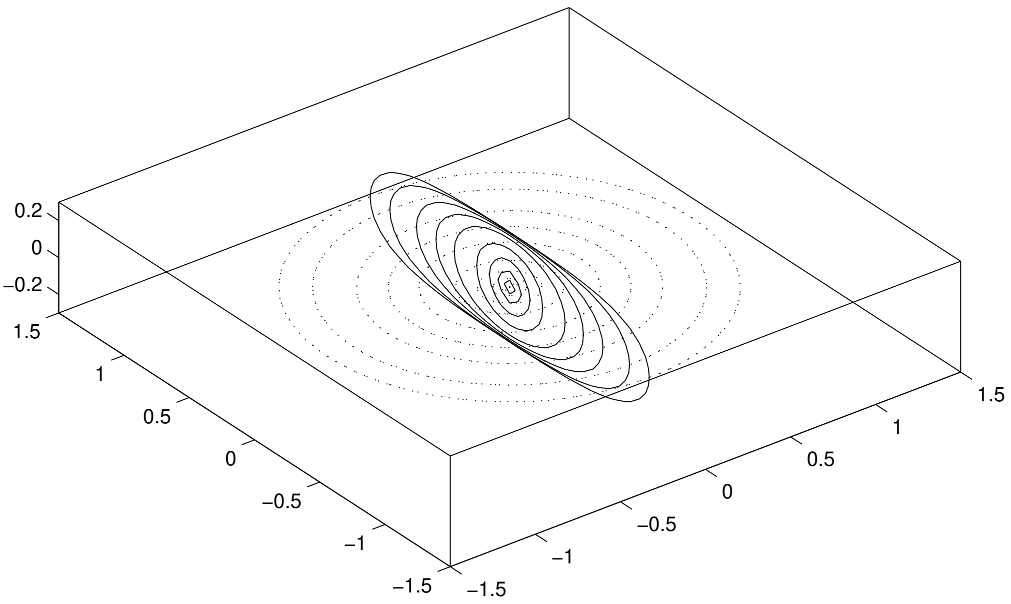

Figure 6: Contour plots on horizontal and vertical cross sections through the centre of the domain Ω^1_{cub} at $\lambda = \lambda_{**}$ with contour levels $0.01, 0.02, 0.05, 0.1, 0.2, 0.5, 1, 2, 5, 10$.

slow in the region $\lambda > \lambda_0$ as $h \to 0$. Thus in Figure 4 we are unable to distinguish visually between the two regions $\lambda < \lambda_0$ and $\lambda > \lambda_0$. Nevertheless, in Section 6.3 we will use the asymptotic theory of Section 5 to obtain good approximations to λ_0.

In Figures 5 and 6 we present numerical computations for the finite element approximation to the solution of (1.1) on the finest mesh in the table at $\lambda = \lambda_{**}$, where we computed λ_{**} in Section 2. In Figure 5 we give surface plots of $U_h(\mathbf{x})$ obtained on two-dimensional cross-sections of the domain by taking a horizontal and a vertical slice through the centre of the domain. The corresponding contour plots are also displayed above the surface. In Figure 6 we display the same two contour plots together, but this time plotted on the relevant cross-sections within the domain. We observe that a narrow peak has developed as predicted. Note that this solution has a high degree of radial symmetry close to the centre of the domain where the singularity is developing. The formal asymptotic theory presented in [7] links such radial symmetry closely with McLeod's conjecture.

6.2 Numerics on a long thin domain: Ω^2_{cub}

In this section we present numerical computations for the full nonlinear problem (1.1) on the domain Ω^2_{cub} with $X = \sqrt{200/299}$ and $Z = 10$ for which Z is now rather larger than Z. Again, we use a fixed topologically regular meshes with cuboid elements all of whose edges are aligned with the coordinate axes. We take regular spaced nodes in the xy-plane for all meshes. On the 4 finest meshes we take the same regular spacing in the z-direction over the central core of the domain to give a regular cubic mesh over the centre of the domain. Over the rest of the domain we also take a regular but coarser spacing of the nodes to give coarser cuboid elements. Since the lengths of the sides of Ω^2_{cub} are not rationally related we cannot take a regular cubic mesh over the domain for our coarse meshes. Thus for the coarser meshes (with the exception of the coarsest mesh) we again take a regular cubic mesh over the centre of the domain, and take elements of approximately the same size over the rest of the domain. The meshes uses are given in the following table.

Core	Core Mesh	Core h	Complete Mesh	'h'
$0.817861 \times 0.817861 \times 10$	$10 \times 10 \times 100$	0.1	–	–
$0.817861 \times 0.817861 \times 0.817861$	$20 \times 20 \times 20$	0.04089	$20 \times 20 \times 240$	0.04174
$0.817861 \times 0.817861 \times 0.817861$	$30 \times 30 \times 30$	0.02726	$30 \times 30 \times 370$	0.02726
$0.817861 \times 0.817861 \times 0.817861$	$40 \times 40 \times 40$	0.02045	$40 \times 40 \times 480$	0.02087
$0.817861 \times 0.817861 \times 0.817861$	$50 \times 50 \times 50$	0.01636	$50 \times 50 \times 450$	0.02296
$0.817861 \times 0.817861 \times 0.817861$	$60 \times 60 \times 60$	0.01363	$60 \times 60 \times 300$	0.03826
$0.817861 \times 0.817861 \times 0.817861$	$70 \times 70 \times 70$	0.01168	$70 \times 70 \times 220$	0.06121
$0.817861 \times 0.817861 \times 0.817861$	$80 \times 80 \times 80$	0.01022	$80 \times 80 \times 180$	0.09182

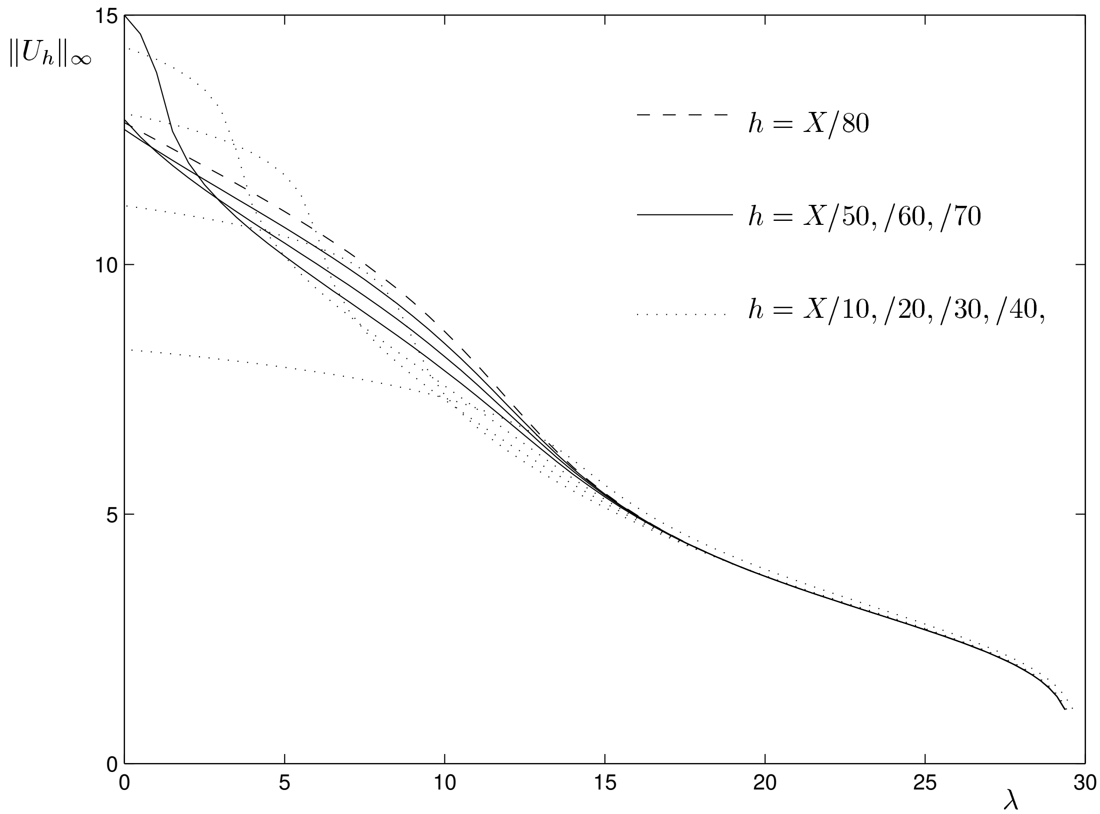

Figure 7: Graph of $\|U_h\|_\infty$ against λ for various meshes (where $X = \sqrt{200/299} = 0.817861$) on the domain Ω^2_{cub}.

The first column of the table gives the size of the central core of the domain on which we use a cubic mesh, the second column gives the mesh used on this central core displayed as the number of elements in each coordinate direction, and the third column the resulting mesh size h across the core. The four coarsest meshes are approximately regular with approximately cubic elements. The fourth column gives the mesh used across the whole domain, again displayed as the number of elements in each coordinate direction, and the final column gives the mesh size h given as the largest length of a side of an element. Thus for example, the fifth mesh has two different shaped elements; all elements in the central core are cubic of side length 0.01636, whilst all other elements are $0.01636 \times 0.01636 \times 0.02296$. Once again, on the finer meshes this results in elements with progressively worse aspect ratios, but as Section 6.1 this does not affect the computation. Finally, note that again as in Section 6.1, there are two different measures of h in the table, with the first value of h for the central portion of the domain governing the asymptotic convergence theory of Section 5, and the second value being a measure of the mesh size.

In Figure 7 we plot the infinity norm of the numerical solution U_h against λ on various meshes. The resulting graph has a similar structure to Figure 4 for the domain Ω^1_{cub} and to the graphs in [7] for the cube. Note that, similar to Ω_1, on the course meshes there is little agreement between the numerical solutions on the different meshes for $\lambda \leqslant 18$, whilst on the finer meshes there is better agreement for $13 \leqslant \lambda \leqslant 18$ whilst for lower values of λ it appears that $\|U_h\|_\infty$ is increasing monotonically as h is refined. Again, as in the case of Ω^1_{cub}, we are unable to distinguish visually between these two regions $0 \leqslant \lambda < \lambda_0$ where (1.1) has no solution, and the region $\lambda > \lambda_0$ on which U_h is converging to the exact solution of (1.1). Nevertheless, in Section 6.3 we will use the asymptotic theory of Section 5 to obtain good approximations to λ_0.

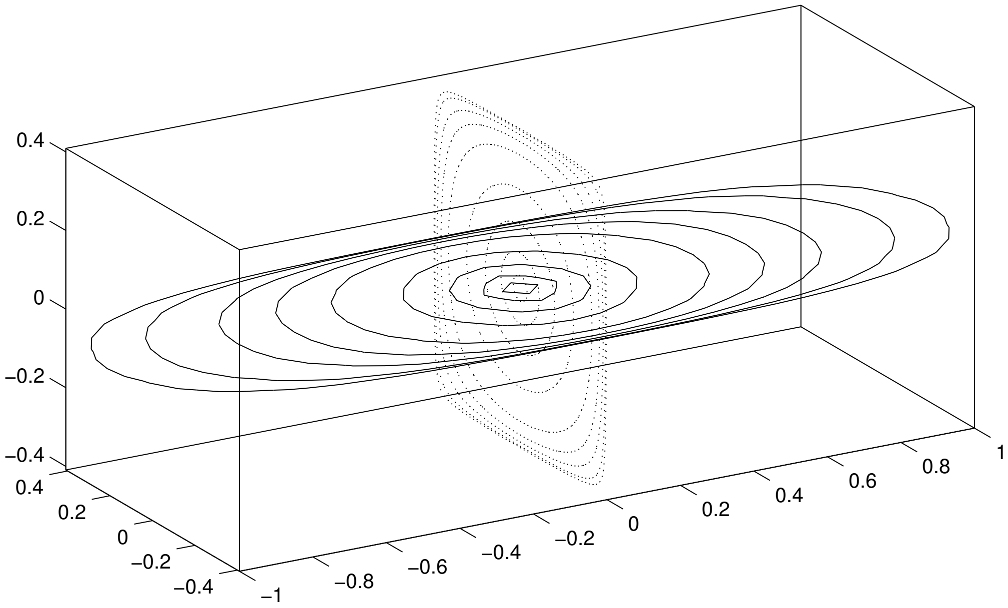

Figure 9: Contour plots on horizontal and vertical cross sections through the centre of the domain Ω^2_{cub} at $\lambda = \lambda_{**}$ with contour levels $0.01, 0.02, 0.05, 0.1, 0.2, 0.5, 1, 2, 5$.

In Figures 8 and 9 we present numerical computations for the finite element approximation to the solution of (1.1) on the finest mesh in the table at $\lambda = \lambda_{**}$, where we computed λ_{**} in Section 2. In Figure 8 we give surface plots of $U_h(\mathbf{x})$ obtained on two-dimensional cross-sections of the domain by taking a horizontal and a vertical slice through the centre of the domain. The corresponding contour plots are also displayed above the surface. In Figure 9 we display the same two contour plots together, but this time plotted on the relevant cross-sections within the central portion of the domain. Again we see a high degree of radial symmetry close to the centre of the domain.

6.3 Post-processed Numerical Solutions

Using the asymptotic theory of Section 5 we can post-process our finite element solutions to obtain better approximations to the solution u of (1.1). Taking the formulae (5.3) we obtain Figures 10 and 11 for the extrapolated values of γ^* for the domains Ω^1_{cub} and Ω^2_{cub} respectively.

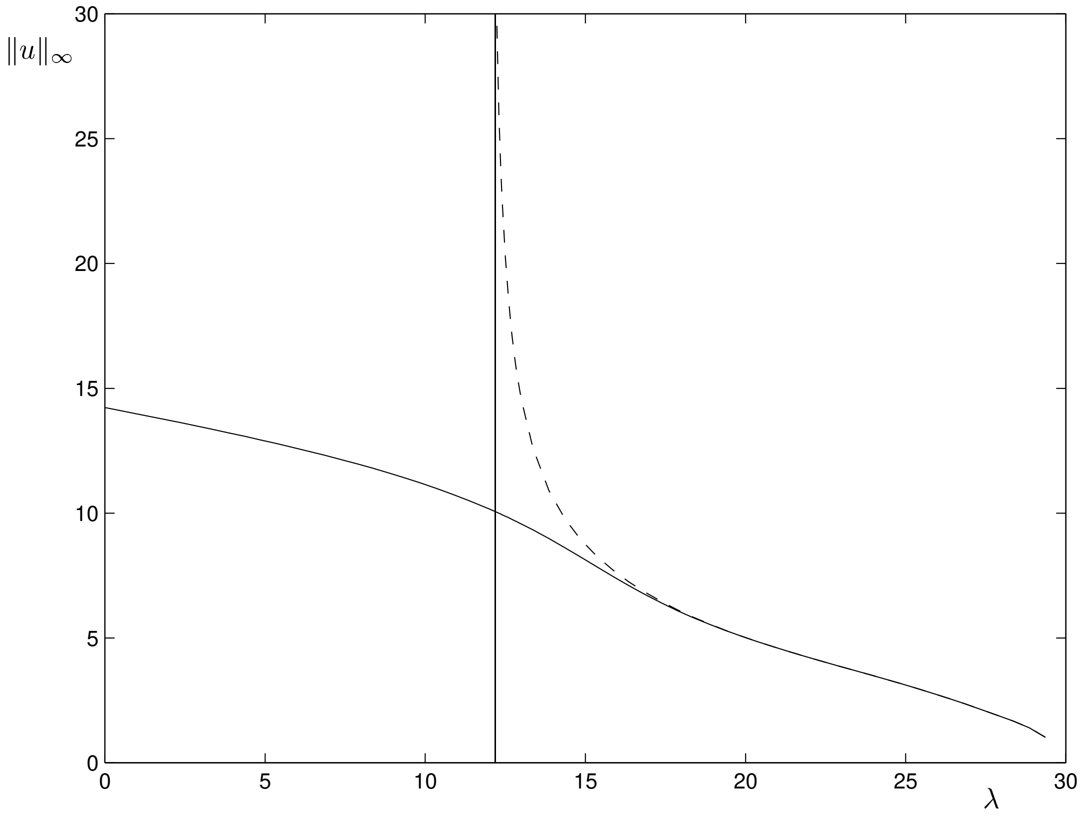

Figure 10: Graph of $\|U_h\|_\infty$ and the post-processed infinity norm against λ with λ_{**} also marked, for the domain Ω^1_{cub} with $h = 0.6/80$.

Note that for both these domains bounded positive solutions U_h for the finite element approximation to (1.1) continue to exist for values of $\lambda < \lambda_{**}$, however the infinity norm of the processed numerical solution becomes large at a value of λ very close to λ_{**}, suggesting that $\lambda_0 = \lambda_{**}$. The discrepancy here is very likely due to higher order errors in the asymptotic formulae. Similar results have already been presented in [7] for the cube.

Since we expect $\|u\|_\infty$ to become unbounded at the values of λ for which the denominator of the right hand-side of (5.3) vanishes, we can modify our finite element program to perform interval bisection to find the value of λ such that

$$\lambda = Ch^2\|U_h\|^8_\infty \tag{6.1}$$

which gives us a numerical approximation to λ_0. In the following table we display results $\lambda_0(h)$ for the domain Ω^1_{cub} (on the $h = 0.6/80$ mesh described in Section 6.1), the domain Ω^2_{cub} (on the $h = 0.81786082/80$ mesh described in Section 6.2) and on the unit cube with a regular mesh of size $h = 1/80$, together with the previous computed values of λ_{**} and λ_{***}.

Domain	$\lambda_0(h)$	λ_{**}	λ_{***}
$\Omega_1 = 3 \times 3 \times 0.6$	11.9986	12.1813	13.1640
$\Omega_\square = 1 \times 1 \times 1$	7.42225	7.50383	7.53445
$\Omega_2 = \sqrt{200/299} \times \sqrt{200/299} \times 10$	9.25307	9.37161	9.62236

Clearly the computed value of $\lambda_0(h)$ is closer to λ_{**} than to λ_{***} and these computations lead us to believe that $\lambda_{**} = \lambda_0$. The difference the computed values of $\lambda_0(h)$ and λ_{**} we

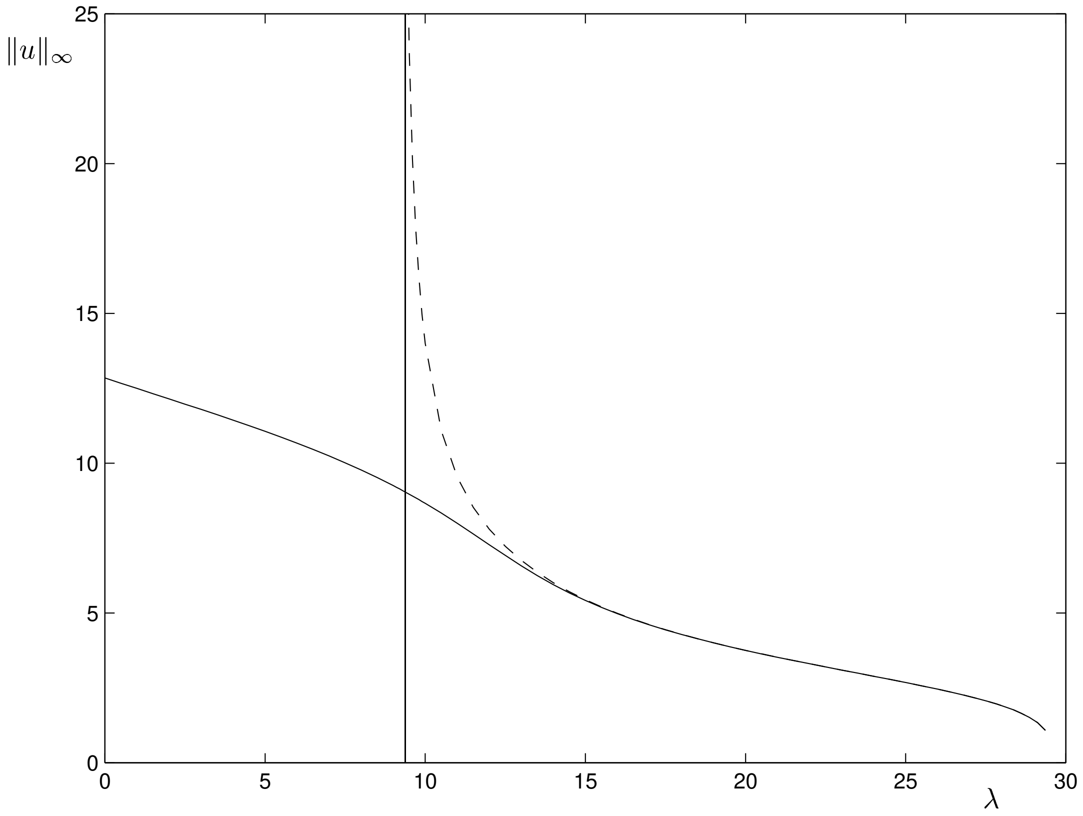

Figure 11: Graph of $\|U_h\|_\infty$ and the post-processed infinity norm γ^* against λ, with λ_{**} also marked, for the domain Ω^2_{cub} with $h = 0.81786082/80$.

believe arises from two sources in the computation of $\lambda_0(h)$. Firstly, from the neglected terms in the asymptotic analysis of Section 5 which leads to (5.3), and secondly, due to computational limitations, from our application of this formula to meshes with h only moderately fine. Recall that the computed value of λ_{**} comes from the solution of a linear problem and is thus highly accurate.

Finally we investigate the dependence on the estimated value $\lambda_0(h)$ of λ_0 on the mesh size h. To do this, we compute $\lambda_0(h)$ as above for the unit cube $\Omega_\square$ on regular meshes $h = 1/10, 1/20, \ldots$.

$1/h$	$\lambda_0(h)$
10	12.35761
20	9.36494
30	8.32328
40	7.87946
50	7.65899
60	7.53778
70	7.46637
80	7.42225
90	7.39412
100	7.37586

Clearly (5.3) is inaccurate for large values of $h > 1/50$, but the values appear to be converging on the finer meshes. This value is lower than the calculated value of λ_{**}. A more careful calculation based upon the results in [7] implies that the value of Γ becomes infinite when

$$\lambda = Ch^2\|U_h\|_\infty^8 \left(1 + \mathcal{O}\left(h^2\|U_h\|_\infty^4\right)\right).$$

At λ_0 we also have from the results of section 5 that

$$h^2\|U_h\|_\infty^4 \approx 60h.$$

Even for the finest meshes considered, this error term is not especially small and certainly consistent with the difference between the numerical estimate and that of λ_{**}. We contrast this with the estimate for λ_{**} and λ_{***} which is far more accurate.

7 Conclusions

We have presented both numerical and analytic estimates for λ_0, λ_{**} and λ_{***} for a variety of regular star-shaped domains. These results are consistent (up to the errors in the numerical calculations) with the result that

$$\lambda_0 = \lambda_{**} < \lambda_{***}$$

for domains other than the ball. At present we seem to be at the limit of computational accuracy for these domains. For a further investigation we propose to investigate less regular domains which are not star-shaped and to consider the validity of the conjectures in these cases as well.

Acknowledgement

The authors are grateful to Andy Wathen for useful discussions and aid in implementing the finite element method.

References

[1] M. Abramowitz and I.A. Stegun. *Handbook of mathematical functions with formulas, graphs and mathematical tables.* Applied Mathematics series. U.S.G.P.O., Washington, 1964.

[2] C. Bandle and M. Flucher. Harmonic radius and concentration of energy; hyperbolic radius and liouville's equations $\Delta U = e^U$ and $\Delta U = U^{\frac{n+2}{n-2}}$. *SIAM Review*, 38:191–238, 1996.

[3] H. Brezis. Elliptic equations with limiting Sobolev exponents – the impact of topology. *Comm. Pure Appl. Math.*, 39:S17–S39, 1986.

[4] H. Brezis and L. Nirenberg. Positive solutions of nonlinear elliptic equations involving critical Sobolev exponents. *Comm. Pure Appl. Math.*, 36:437–477, 1983.

[5] C.J. Budd and A.R. Humphries. Adaptive methods for semilinear elliptic equations with critical exponents and interior singularities. *Appl. Numer. Math.*, 26:227–240, 1998.

[6] C.J. Budd and A.R. Humphries. Weak finite dimensional approximations of semi-linear elliptic PDEs with near critical exponents. *Asymptotic Analysis*, 17:185–220, 1998.

[7] C.J. Budd, A.R. Humphries, and A.J. Wathen. The finite element approximation of semi-linear elliptic PDEs with critical exponents in the cube. *SIAM J. Sci. Comp.*, 20:1875–1904, 1999.

[8] I.S. Gradshteyn and I.M. Ryzhik. *Table of integrals, series and products.* Academic press, 1980.

[9] B. McLeod. A nonlinear elliptic equation with critical Sobolev exponent, 1984. Unpublished work.

[10] Numerical Algorithms Group. *NAG Fortran Library manual*, 1990.

[11] R. Piessens, I. Mertens, and M. Branders. Integration of functions having endpoint singularities. *Angewandte Informatik*, 16:65–68, 1974.

[12] R. Schoen. Conformal deformation of a Riemannian metric to constant scalar curvature. *J. Diff. Geom.*, 20:479–495, 1984.

[13] S. Wang. The existence of a positive solution of semilinear elliptic equations with limiting Sobolev exponent. *Proc. Roy. Soc. Edinb.*, 117A:75–88, 1991.

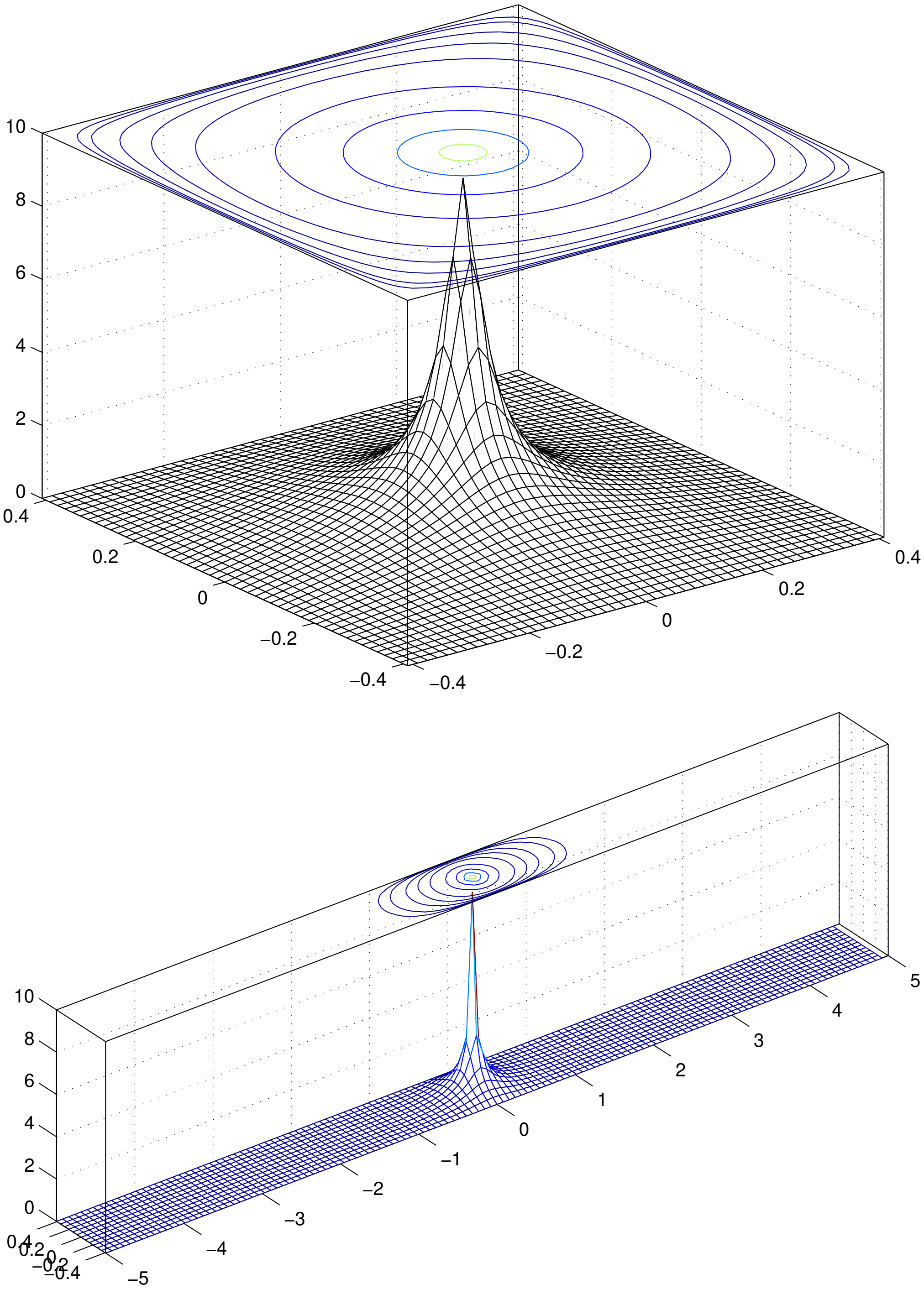

Figure 8: Two cross sections of U_h through the centre of the domain Ω^2_{cub} at $\lambda = \lambda_{**}$ and contour plots (with contour levels $0.01, 0.02, 0.05, 0.1, 0.2, 0.5, 1, 2, 5$); (i) through $z = 5$, (ii) through $x = \sqrt{50/299}$.

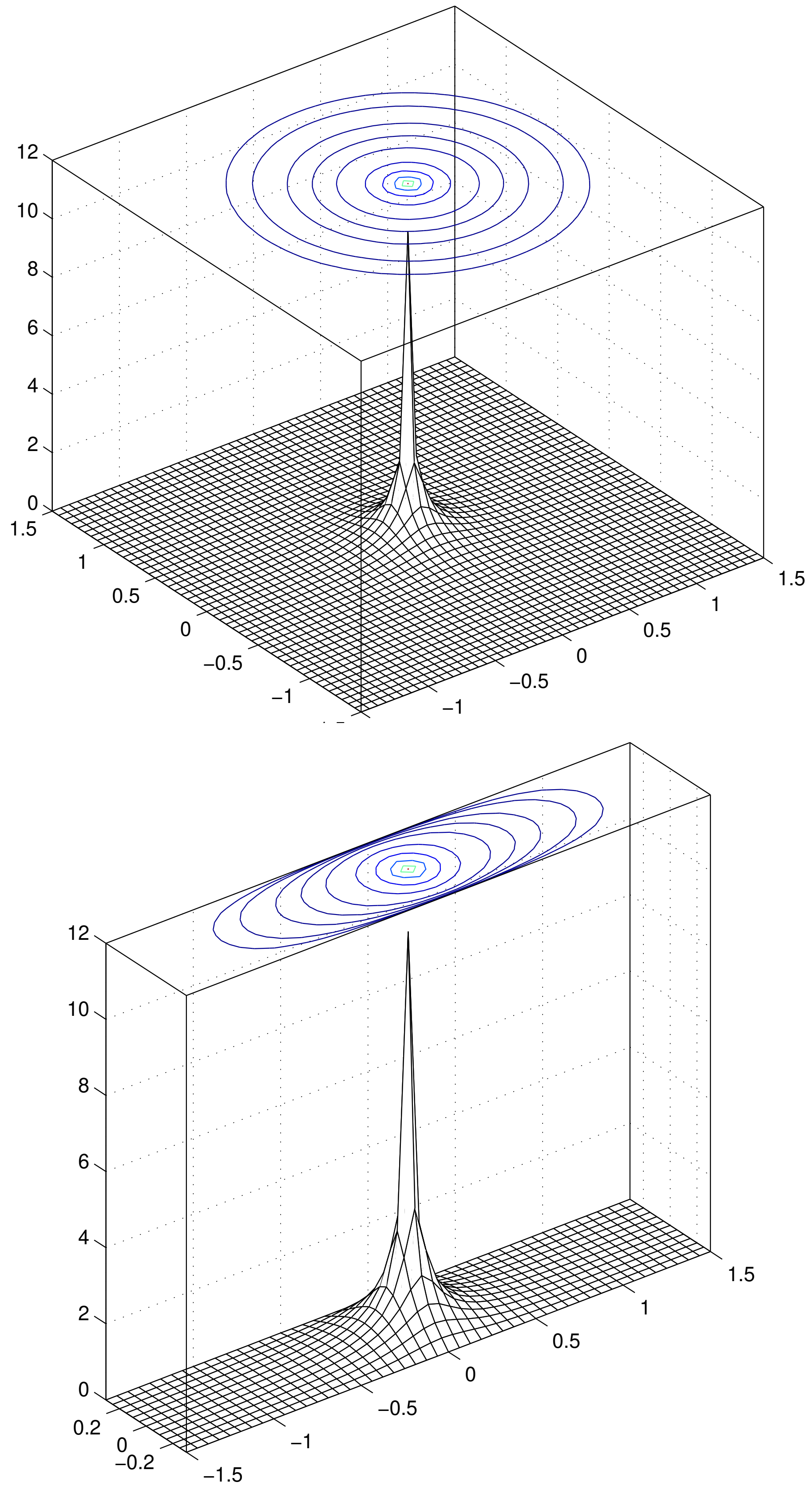

Figure 5: Two cross sections of U_h through the centre of the domain Ω^1_{cub} at $\lambda = \lambda_{**}$ and corresponding contour plots (with contour levels $0.01, 0.02, 0.05, 0.1, 0.2, 0.5, 1, 2, 5, 10$); (i) through $z = 0.3$, (ii) through $x = 1.5$.